

See discussions, stats, and author profiles for this publication at: <https://www.researchgate.net/publication/48180123>

Characterisation of spatial network-like patterns from junctions' geometry

Article · January 2011

Source: arXiv

CITATIONS

2

READS

346

3 authors:



Andrea Perna

IMT School for Advanced Studies

86 PUBLICATIONS 1,820 CITATIONS

SEE PROFILE



Pascale Kuntz

University of Nantes

212 PUBLICATIONS 2,955 CITATIONS

SEE PROFILE



Stéphane Douady

French National Centre for Scientific Research

193 PUBLICATIONS 6,628 CITATIONS

SEE PROFILE

Large scale coherence of spatial network-like patterns identified using local geometry.

Andrea Perna^{1,2,4}, Pascale Kuntz², Stéphane Douady³

¹ *Institut des Systèmes Complexes Paris Île-de-France, 57-59 rue Lhomond, F-75005, Paris, France*

² *École Polytechnique de l'Université de Nantes, 19 rue Christian Pauc, BP50609, 44306 Nantes, France*

³ *Laboratoire Matière et Systèmes Complexes UMR 7057,*

Bâtiment Condorcet Université Paris Diderot - CC7056, 75205 Paris cedex 13, France

⁴ *Mathematics Department, Uppsala University, Box 480, 75106 Uppsala, Sweden*

We propose a new method for quantitative characterization of spatial network-like patterns with loops, such as surface fracture patterns, leaf vein networks and patterns of urban streets. Such patterns are not well characterized by purely topological estimators: also patterns that both look different and result from different morphogenetic processes can have similar topology. A local geometric cue -the angles formed by the different branches at junctions- can complement topological information and allow to quantify the large scale spatial coherence of the pattern. For patterns that grow over time, such as fracture lines on the surface of ceramics, the rank assigned by our method to each individual segment of the pattern approximates the order of appearance of that segment. We apply the method to various network-like patterns and we find a continuous but sharp transition between two classes of spatial networks: *hierarchical* and *homogeneous*. The first results from a sequential growth process and presents large scale organization, the latter presents local, but not global scale organization.

PACS numbers: 89.75.Fb 89.75.Hc 47.54.-r

I. INTRODUCTION

A central issue in complex systems research is to understand the formation and the properties of spatio-temporal patterns found in physics and biology. To this end, an essential step involves obtaining appropriate measures of their form: quantitative estimators that allow to compare different patterns and to validate objectively models. This paper focuses on the family of spatial patterns that are "network-like".

Network-like patterns are common in natural and artificial systems: they are found in leaf veins, fractures on the surface of materials, patterns of urban streets and animal trails, galleries, river networks, blood vessels and circulatory systems. The factors underlying the formation of these patterns are different from system to system: surface cracks result from the shrinkage and stress of materials; urban streets are generated by human activity and so on. In spite of intrinsic differences a few simple morphogenetic events describe the formation of all these patterns: nucleation of new network components, elongation of existing segments, branching and intersection. The final topology of the pattern is completely determined by the sequence of such growth events, plus a pruning event: the cut or removal of already formed segments.

Many studies have used topological estimators to describe the form of net-like patterns and better understand their morphogenesis and functional properties. One of the first progresses in this direction goes back to the Horton-Strahler coefficients, introduced in the forties by the hydrogeologist Robert E. Horton [1] as a method to describe quantitatively the form of rivers and of their hydrologic basins. Such coefficients became particularly popular in the improved formulation by Strahler [2]. In

this formulation, the uppermost streams of a river are given rank 1 and the rank of other branches is derived by iterating a local rule: whenever two streams with the same rank N merge together, they originate a stream with rank $N + 1$; conversely when a stream with rank $N + 1$ receives the input of a lower order stream (rank $\leq N$) its rank is unchanged. Horton-Strahler's method is a simple but powerful tool to describe quantitatively the form of hydrogeologic networks and allowed to study the scaling relationships between different parts of the river. The method was applied to the study of such different systems as river networks [3–5], leaf patterns [6], and even ant trail patterns [7]. Unfortunately, Horton-Strahler's ranking method cannot be applied to networks with cycles. This has a profound impact on the applicability of the method, as many real-world network-like patterns have cycles.

General graphs are characterized by a whole set of measures of the local and global organization: node degree, assortativity between nodes, clustering coefficient, frequency of specific subgraphs, presence and number of cycles, diameter, path length etc. [8–10]. Several studies have computed graph measures and used them to quantify the local and large scale organization of real world spatial patterns, such as urban street patterns [11–19], systems of animal trails [20] and galleries [21–25], networks of channels in trabecular bones [26, 27], networks of fungal ifae [28].

Unfortunately, purely topological estimators, however useful, do not fully account for the organization of 2D net-like patterns which present specific constraints. For instance, in planar graphs, the average node degree cannot be higher than six. In addition, for a number of net-like patterns, the degree distribution is even more regular than what is imposed by planarity: the great majority

of nodes is found to have degree equal to three in such different systems as two-dimensional foams [31], honeycomb patterns and biological epithelia [32], leaf vein networks [33], fracture patterns [34]. In self-organized, “bottom-up” towns [11, 14] the majority of junctions between streets also have degree three (though the same does not hold for planned towns, where the majority of crossroads have degree four [14] or even higher [35]). The homogeneity of degree is reflected (as a consequence of Euler formula) into a homogeneity in the length of network cycles that are composed by six edges on average in all the aforementioned systems. Similarly, network distances are not much informative as they basically scale with euclidian distances in all these systems.

Here we want to use the spatial information to provide a deeper understanding of the pattern. We focus in particular on the information carried by the angles formed at junctions. This choice is motivated by two complementary arguments, one about the physics of the growth of the network-like pattern, which can influence directly the branching angles, and the other about dynamic properties (e.g. navigation) that may take place on the resulting network.

Throughout the text, we will make extensive use of the words *edge* and *segment* with the following definitions: an edge is the linear structure between two consecutive junctions (classical network edge) and a segment is a contiguous unbranched series of network edges grouped together as described later in section II, that reveals the larger scale structure.

A. growth

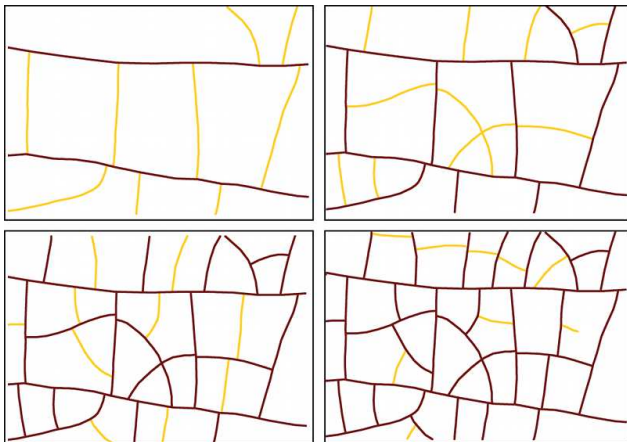


FIG. 1: Drawing of the evolution of a fracture pattern in a solution of latex particles [36]. In each image, the light colour indicates the newly appeared fractures. When new lines of fracture appear their growth is affected by the already existing fractures (for instance, newer fractures do not cross older ones). On the contrary, the position of older lines does not change after the appearance of the new ones.

A number of network-like patterns form as the result of a sequential process, where new segments appear at different times [34] without undergoing further reorganization. One example of such patterns is provided by the fracture lines on the glaze of ceramics illustrated in fig. 1. Bohn et al. [34] suggested that urban streets patterns fall into this same morphological class.

The appearance, elongation and termination of new segments is affected by the older segments; the older segments, however, do not undergo further reorganization after the appearance of new ones. Under these conditions (sequential process, growth with no deletion of edges and absence of reorganization) the temporal hierarchy in the appearance of segments is reflected into the spatial hierarchy of lengths and arrangements of the final pattern [36]. Across a junction, as a consequence of this fact, the edges belonging to the older segment are the straight continuation of one another; conversely, the edge belonging to the newer segment form a large angle with the others.

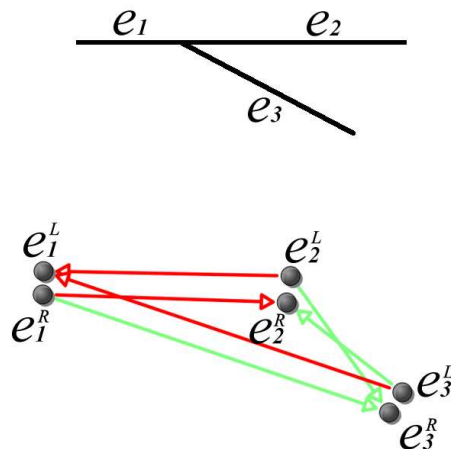


FIG. 2: **A:** Small graph, involving a single junction. **B:** The weighted directed line graph built from the graph in A. Weights are as follows: dark-red \rightarrow weight=0; light-green \rightarrow weight=1

But the local angle information is not sufficient in itself. Considering the case of a junction like the one in figure 2-A, the attribution of edges around the junction to the same or a different segment would be simple in the absence of any information: the most natural inference is to group edges e_1 and e_2 into the same, older, segment. The attribution is more problematic if one already knows that e_3 is older: than it would be more natural to group e_3 and e_1 into the same old segment, and assume e_2 appeared later. In summary, the best inference about what

network edges should be grouped into the same segment depends on the continuity between adjacent edges, but also on the information already available about the order of appearance of other segments. It can then be constructed only sequentially.

B. navigation

When the network-like pattern is also the support for a transportation function, as it is for instance the case with patterns of urban streets, the angles of edges at intersections and junctions will play a role for navigation and orientation.

In architecture, this concept has been theorized in particular under the name of “space syntax” in the work of Hillier and Hanson [37]. With the space syntax method, urban street patterns are fragmented into a number of straight segments (ideally the maximum number of segments in which the line of view is conserved) and one analyses the network obtained representing straight segments as nodes, and where there is an edge if the corresponding straight segments intersect the one another. Then selecting a line (a street) as a starting point, one can number each line in the map according to how many changes of direction separate it from the starting line. This measure is generally referred to as depth and is a kind of distance: it represents the minimum number of changes of direction to go from the origin to any other place in the street network. This kind of measure has been correlated with different aspects of social life, and in particular patterns of pedestrian movement in cities, but also urban traffic, property value and so on [38]. Nevertheless, the process of fragmenting street patterns into segments with the same line of sight was not proven to always have a simple solution and it might be too sensible to small differences of orientation of the urban grid ([39]).

In physics literature, analogous ideas are followed through what is usually called a “dual network” approach (though a more appropriate definition would be “line network” approach), where named streets [17, 40, 41] or contiguous segments [15] are mapped into network nodes and there is an edge whenever two streets intersect or bifurcate. Dual networks also provide a convenient representation for measuring the amount of information necessary to navigate inside the network [40], in particular for navigation strategies relying more upon the continuity of linear elements than on salient points.

In fact one can imagine to describe a path through the network with instructions with the form: “go straight for N steps (N junctions or crossroads), or until you find a salient point (a traffic light, a square...)”, followed by information on which new direction to take. In general a “simple” path will be one that involves only few deviations from the current direction, not necessarily a short one. However, the result will not be the same depending on the direction followed. Let’s illustrate this with ref-

erence to the junction of figure 2-A. Moving from edge e_1 to e_2 , or in the opposite direction from e_2 to e_1 does not involve any change of direction. Going from e_1 to e_3 requires one change of direction (i.e. to abandon the straightest path and take an alternative one), but the opposite is not true since e_1 is the more direct continuation of movement when coming from e_3 .

Both the arguments, about growth and about navigation, illustrate the interest of a representation of network-like patterns that classifies network edges using information provided by angles at junctions. Our examples indicate that the process is not symmetric with the starting point used for classification.

In the following section we introduce a simple algorithm that given a local rule (namely an evaluation of the angles at each junction) and a set of arbitrarily chosen root edges, assigns a rank (expressed by an integer number) to each edge of the network-like pattern. Contiguous edges with the same rank can then be grouped together into segments. The numbers of segments for each given rank and their average properties provide a quantitative statistical characterization of the morphology of the pattern.

The paper is organized as follows. The algorithm is described in detail in section II. In section III we explore the theoretical distribution of ranks and segment lengths on simple lattice models. Possible applications to the understanding of real world spatial networks, as well as the most important limitations are explored in the remaining sections IV to VII.

II. ALGORITHM DESCRIPTION

The computation of the segment numbering is in two steps. First, given a root edge, or a set of root edges, a rank is assigned to each edge. Then, the contiguous edges with the same rank are grouped into segments.

A. computing edge ranks

Given a root edge e_r , the rank of an edge e_i expresses the minimum number of direction changes, meaning not taking the straightest segment, needed to reach e_i when coming from e_r . We can also take into account a set S_r of root edges; in this case, the rank of e_i is the minimum number of direction changes when coming from the closest root edge of S_r .

Again, the propagation of ranks across a junction depends on the direction in which the junction is traversed. For instance, in the graph of figure 2-A if we set the rank of edge e_1 to zero ($rank(e_1) = 0$ by convention), then the rank of e_3 is equal to 1 ($rank(e_3) = 1$), but the same relation does not hold in the opposite direction: if we set the rank of e_3 to zero ($rank(e_3) = 0$ by convention), then the rank of e_1 is also equal to zero ($rank(e_1) = 0$;

no deviation from previous direction when going from e_3 to e_1).

Generally speaking, each edge e_i can be crossed in two directions; by convention, we denote e_i^R (resp. e_i^L) the arc associated to e_i when it is crossed from the right (resp. from the left). To make the computation of all the ranks easier, we consider the dual directed graph G_D (fig 2-B) which models the connections between all the arcs. The vertices of G_D are the arcs $\{e_i^R, e_i^L\}$ associated to any edge of the initial graph, and two vertices e_i^* and e_j^* (the star means either R or L) are linked together in G_D if the extremity of e_i^* is equal to the origin of e_j^* .

For instance, the crossing of the path $e_1 - e_2$ from the left is modeled by $e_1^L \rightarrow e_2^L$ in G_D , and the crossing in the opposite direction by $e_1^R \leftarrow e_2^R$. There is no connection between e_1^L and e_2^R as the navigation $e_1 \rightarrow e_2$ is not directly possible.

Weights are assigned to the arcs of G_D as follows. The weight $w(e_i^*, e_j^*)$ is equal to 0 when the path formed in the initial graph by the edges e_i and e_j is the straightest and 1 otherwise. We can also introduce a threshold on the maximum angle, implying that if the change in direction is too large, then the weight is 1 even if the angle is the minimum one. Formally, $w(e_i^*, e_j^*) = 0$ when (1) the angle formed in the initial graph by e_i^* and e_j^* is the minimum angle formed by e_i^* and its adjacent vertices, and (2) this angle is smaller than a given threshold (in our analysis chosen to be 45 degrees).

Once defined a root edge e_r in the initial graph whose rank is equal to 0 by convention, the ranks of the other edges can be easily obtained by a distance computation in G_D : the rank $rank(e_i)$ of any edge e_i is defined by

$$rank(e_i) = \text{Min} \{d(e_r^L, e_i^L), d(e_r^L, e_i^R), d(e_r^R, e_i^L), d(e_r^R, e_i^R)\}$$

where d is the shortest path distance in the dual directed graph G_D weighted by w . When a set S_r of root vertices is fixed, the rank of e_i is the minimum of the ranks computed from all the edges of S_r with the above formula.

B. grouping edges into segments

Several adjacent edges with the same rank can be grouped together into “segments”. A segment is a series of edges all having the same rank and with exactly two ends (not including junctions). The segment is initialized with any edge of G . Its continuation is determined by pairing together adjacent edges of the same rank until one of the following conditions is encountered:

1. There are no more edges with the same rank at one extremity.
2. The segment intersects an edge of lower rank.

In the special case when three or more edges with the same rank are incident to the same junction, the continuation of the segments is determined by pairing together

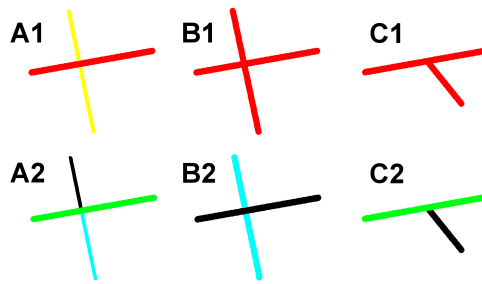


FIG. 3: Illustration of the procedure for grouping together edges into segments. **A1**: the near-horizontal edges have lower rank than the near-vertical edges. The edges are grouped in **A2** into three segments: a near-horizontal lower rank segment and two segments with higher rank. **B1**: all the edges have the same rank. In this case, two straight segments are identified in **B2**. If an odd number of segments with the same rank meet at a junction (**C1**), the one that deviates more from the direction of the others forms a distinct segment (**C2**).

the two edges that provide the straightest continuation of one another, then we proceed pairing together all the other edges incident to the node in a similar way. If an odd number of edges with the same rank meet at a junction, one edge remains excluded from all the pairings and the segment comprising that edge is terminated at the junction.

We can give an intuitive justification for the above rules. Imagine the case of a network-like pattern resulting from a sequential growth process, such as for instance fracture lines on ceramics. Grouping edges into segments is equivalent to identify those network edges that belong to the same line of fracture. With condition 2 we impose that younger lines of fracture (higher ranks) never cross already formed fracture lines. A parallel can also be found with what happens for urban street patterns, where small streets usually change their name when crossing larger ones.

Figure 3 shows examples of how segments are grouped together. In A1 the near-horizontal edges have lower rank than the near-vertical edges. In this case, the near-vertical edges form two distinct segments (A2), in spite of being in direct continuity. B1 presents exactly the same pattern, except that now all the edges have the same rank. In this case, the edges are grouped together in two intersecting segments, one near-horizontal and one near-vertical (B2). When there is an odd number of edges intervening at a junction, as in C1, the couple(s) of edges that deviate less from each other direction are paired together in the same segment(s) and the remaining edge form a segment by itself, that is ended at the junction (C2).

To summarize, the straight contiguity of edges is well represented by a directed line graph LG_d whose arcs are weighted with appropriately chosen weights. The arbitrary selection of a set of root edges in G allows to express changes of direction in terms of a distance mea-

sure, allowing to assign each edge of G a rank number. Edges that are more likely to belong to the same spatio-temporal event of network formation can be grouped together into segments.

III. LATTICE MODELS

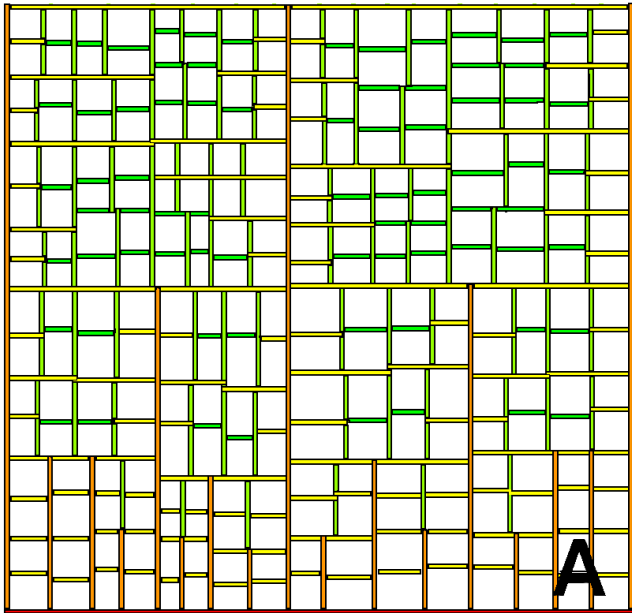


FIG. 4: Mondrian pattern generated by iterated domain divisions. Here, divisions are alterned: all the cuts operated at division $t+1$ are horthogonal to the cuts at t . In all figures, the color of the edges reflects their rank; a periodic rainbow colormap is used. For this example, all the edges in the bottom of the figure are selected as roots.

In this section we explore the distribution of segment ranks and edge ranks in a simple lattice model. In particular, we introduce a class of lattice models that we call “Mondrian” lattices, intended to mimic the growth process and the characteristics of hierarchical network-like patterns. In order to build the lattice, we start with a single rectangular domain and we iterate the following operation: each rectangular cell of the lattice is divided in two smaller rectangles by introducing a new cut parallel to one of its sides (let’s say horizontal or vertical) at a random position chosen from a normal distribution around its centre. The cuts can either be “alterned”, where horizontal cuts at time t are followed by vertical cuts at time $t+1$, and vice-versa, or “random”, where the horizontal or vertical direction of cut is chosen randomly for each cell and each division.

Here, and in the rest of the paper, we will focus mainly on two kinds of statistics. The first is the histogram of the numbers (or percentages) of *segments* with any given rank. This gives an information on the structuration of the pattern between segments of various orders. The

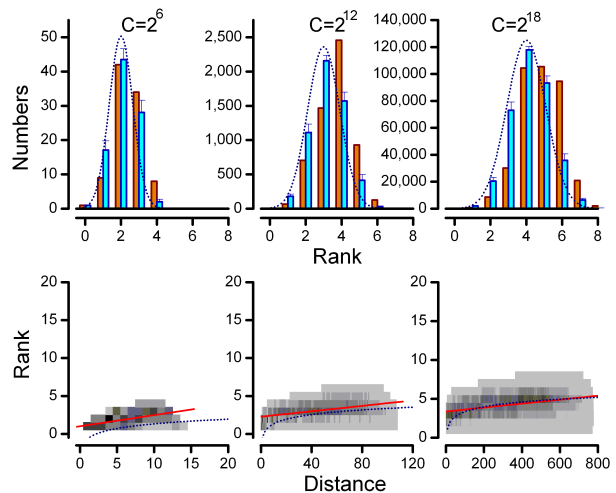


FIG. 5: Top row: histogram of number of segments for Mondrian lattices of different size from left to right 2^6 , 2^{12} , and 2^{18} cells (C). Orange histogram: alterned divisions. Cyan histogram: random divisions. Bottom row: distribution of the same edges for the same alterned Mondrian lattices. Red continuous line: linear fit to the data. The slope is 0.148 for $C = 2^6$, 0.018 for $C = 2^{12}$ and 0.002 for $C = 2^{18}$. Blue dotted line: function reported in equation 2

second measure relies on *edges*, not segments, and looks at how the ranks of individual edges increase with their topological distance from the sources. Intuitively, the rank measures the number of direction change needed to reach a particular edge and the topological distance measures the number of vertices crossed. Hence, $\frac{1}{slope}$ of this curve gives the average length of the straight segments. This can also be seen as the largest scale at which spatial organization is observed.

Figure 5, top row, gives the histogram of the numbers of segments with any given rank for Mondrian lattices after 6, 12 and 18 iterations of divisions. The orange and cyan histograms are for alterned and random divisions, respectively. For random divisions the asymptotic distribution is a Normal distribution $N(x)$ of the form

$$N(x) = A \cdot e^{-\frac{(x-\bar{x})^2}{2\sigma^2}} \quad (1)$$

where $\bar{x} = 2 + \lfloor \frac{(t-2)}{6} \rfloor$ (with t the number of iterations of divisions), $A = \frac{2^{t+1}}{\sqrt{t+1}} \cdot 1.04328$ and sigma $\sqrt{t+1} \cdot 0.25$. In practice, for a pattern observed at a single time, t is usually unknown, and it is easier to approximate t in term of the number of cells C , assuming that it holds the relation $C = 2^t$. The number of cells for planar graphs in turn is easily obtained from the number of edges and vertices in the network through the Euler’s formula for planar graphs, stating that $V - E + C = 1$.

When looking at the ranks of *edges* (instead of segments), one can plot the rank vs. the topological dis-

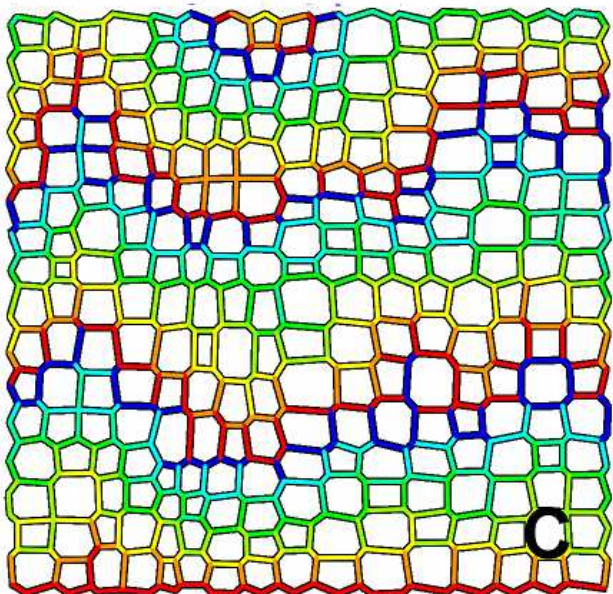
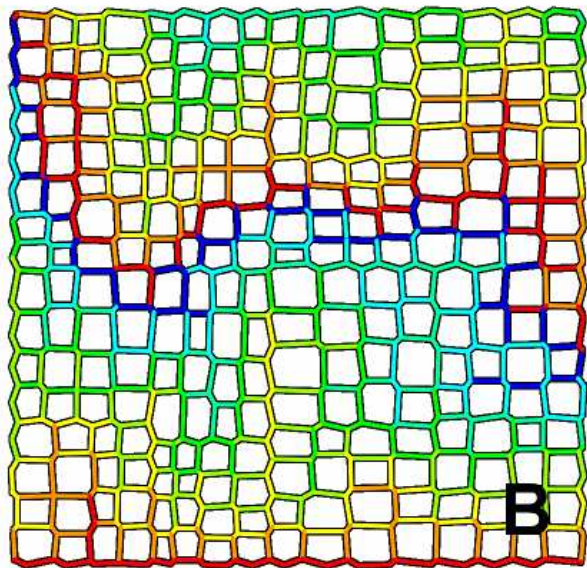


FIG. 6: The same lattice as in figure 4. The positions of each node but those on the perimeter of the lattice is shifted by associating to all its adjacent edges a vector of unitary length and centrifugal direction and computing the vectorial sum over all the adjacent edges. This progressively destroys the large scale organization of the pattern.

tance for each network edge. Figure 5, bottom row, reports this distribution for alterned Mondrian lattices of different sizes (6, 12 and 18 iterations of division), together with a linear fit of the distribution (continuous red line). We can see that when the number of iteration increases the overall slope decreases, revealing in fact a curved relation. More precisely, the dependency of rank vs. physical distance could be fitted by the following

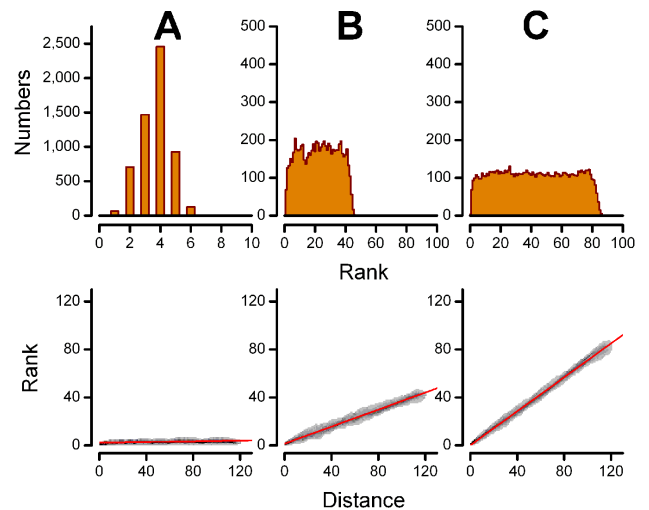


FIG. 7: From left to right: same plots as in the previous figures for three lattices with 2^{12} cells each. The slope of the fit for the bottom figure is 0.014 for A 0.355 for B and 0.707 for C (the slight differences from the lattice with no degradation here and the lattice with 2^{12} cells of figure 5 middle row are due to the additional edges introduced by imposing periodic boundary conditions).

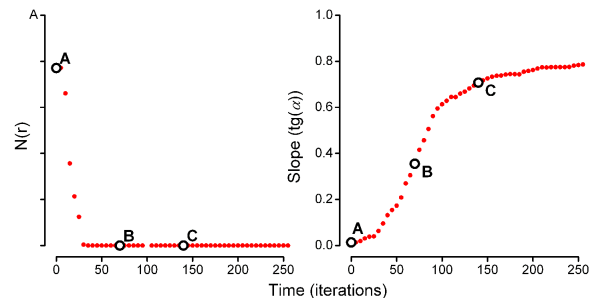


FIG. 8: When the angles at junctions are altered by applying forces to the edges (as shown in figure 6), the global organization of the pattern is rapidly lost. The plots report $N(\bar{r})$ for the segments and $tg(\alpha)$ for the edges of a Mondrian lattice obtained with 12 alterned divisions when the angles formed at junctions are progressively altered (see the main text).

equation for large lattices:

$$rank = \sqrt{\frac{3}{8}} \cdot \log_2(distance) + \log_2\left(\sqrt{\frac{3}{8}}\right) \quad (2)$$

This logarithmic relation is not surprising as distances scale with the logarithm of the number of nodes both in random graphs [29] and small world networks [30].

We assessed the stability of the measured ranks to the local and large scale organization of the lattice by progressively destroying the edge orientations. This should give us a better intuition of the kind of results that we might expect for real world network-like patterns with irregular and noisy organization.

In principle, several strategies for destroying edge contiguity can be imagined. However, if we take inspiration from real patterns we notice that for a number of physical and biological systems network like patterns evolve toward a configuration that achieves a local minimization of the length of the linear structure. Two-dimensional foams [31], honeycombs, biological epithelia, dragonfly wing patterns [32], but also some geological formations such as columnar joints found in basaltic lava rocks [42] all involve roughly hexagonal tessellations of the plane, and symmetric, tripartite junctions. The formation of symmetric tripartite junctions is usually understood as the result of forces directed to minimize the local length of network segments. In fact, the hexagonal pattern is the tessellation that fills the space using the minimum total length of linear segments [43]. The formation of such symmetric configurations can be explained in terms of minimization of forces. The most well-known example of such force models is Lami's theorem (cited e.g. in [32]), which states that if three coplanar forces are acting on a same point and keep it stationary, then it obeys the relation $\frac{A}{\sin(\gamma)} = \frac{B}{\sin(\beta)} = \frac{C}{\sin(\alpha)}$ where A, B and C are the magnitude of forces acting at the point, and the values of α , β and γ are the angles directly opposite to the forces C, B and A respectively.

Such an evolution from horthogonal, Mondrian like, configurations towards more symmetric, foam-like junctions is documented for some real world patterns. For instance, in the case of basaltic lava rocks, the hexagonal pattern was shown to derive directly from tetragonal networks. This process involves the gradual change of orthogonal intersections toward nonorthogonal intersections of about 120 degrees as the joints grow inward during solidification of lava [44, 45]. This is also the case for leaf vein patterns, which first would form as fractures at right angles, but then would evolve continuously with aging towards more symmetric foam-like tripartite junctions [33].

It thus appears a natural choice to use similar rules to progressively destroy the edge contiguity of Mondrian lattice models: Starting from a lattice of 2^{12} cells, obtained through alterned divisions, we iterated the following operation: at each time step the node positions are shifted by computing the resultant of vectors directed along the incident edges and oriented centrifugally. Each vector has magnitude (*sideofthegrid*) $\cdot \frac{1}{30000}$. The interest is to explore the continuity between the two extremes of a Mondrian pattern and a two dimensional foam.

Figure 6 shows two snapshots of a portion of the lattice at different steps of degradation. Figure 7 presents the statistics of segment histograms (top) and edge rank vs. edge distance (bottom) for the three levels of degradation corresponding to the figures 4-A and 7-B and C. When the lattice is progressively degraded, the histogram of segment ranks becomes flat and its center shifts far to the right of the theoretical peak. The slope of edge rank vs. edge distance, that is nearly zero for the original lattice A, increases progressively for the degraded lattices B and C.

We propose two measures for quantifying the distance of a given distribution from the theoretical distributions found with Mondrian lattice (or the level of degradation of edge contiguity). The first quantity is $N(\bar{r})$, where \bar{r} is the mean rank over all the segments of a pattern and $N(\bar{r})$ is the value of the theoretical distribution $N(x)$ normalized to have peak value equal to 1 ($A = 1$ in eq. 1) for a Mondrian lattice with the same number of cells when $x = \bar{r}$. This quantity will be 1 if the mean of the real distribution is equal to the theoretical mean and will fall to zero when the real distribution is far from that of a theoretical Mondrian lattice. The second quantity is the slope $tg(\alpha)$ of the linear least squares fit to the distribution of rank (distance from the root edges measured in number of changes of direction) vs. network distance (distance from the root edges measured in number of interposed edges) $rank = tg(\alpha) \cdot (distance) + r_0$. For large Mondrian lattices $tg(\alpha) \simeq 0$. In fact, while ranks increase with the logarithm of network size, topological distances increase with the square root of network size. When the continuity of straight lines is lost $tg(\alpha)$ will progressively increase, with an upper boundary at 1, when each junction determines the increase of ranks, as e.g. would be the case in hexagonal lattices.

Figure 8 (left) reveals that $N(\bar{r})$ decrease very abruptly, becoming negligible except near the perfect Mondrian Pattern. This show that this measure is very sensitive to the global large scale coherence, that is lost very quickly. The slope (8, right) shows also a continuous transition, but on a larger interval. This means that once the large scale coherence is lost, the coherent length (inverse of the slope), decreases continuously. In other words the first measurement seems like a qualitative measurement of the large scale hierarchical structure, while the second measure is a quantitative measure of the distance to a foam.

In general, real patterns will deviate in various ways from these simple lattice models. In the following of the paper we explore the distribution of ranks and segment statistics in three different examples of real world network-like patterns: the pattern of fracture on the surface of materials, patterns of leaf veins in dicotyledon plants, and the pattern of urban streets in (unplanned) towns.

IV. FRACTURE PATTERNS

Crack patterns often form on the surface of materials as the result of the shrinking of one material layer frustrated by its deposition on a non-shrinking substrate. This kind of pattern formation has been extensively observed and reproduced in controlled settings on a variety of materials, including mud, ceramics, coffee grounds. The final patterns result from the combination of two distinct processes: the nucleation of new fractures on the surface of the material and the propagation of existing fractures [46–48]. Nucleation of new fractures usually



FIG. 9: Edge ranks computed for the fracture pattern of figure 1. The color coding is the same as for other figures. The \square and \circ symbols are referred to in the main text.

involves the formation of tripartite junctions with equal angles of about 120 degrees [48]. Conversely, junctions formed by propagating fractures form as the result of either two fractures meeting at a point (which usually do so with orthogonal angles), or of the branching of one growing fracture (and in this latter case the angles formed at junction are less predictable). If the crack pattern is produced in a non-elastic material, there is no reorganization after its formation and the final form of the pattern reflects the mechanisms of formation. Depending on the characteristics of material, either nucleation of new fractures will be the most frequent process or propagation of already formed fractures over long distances. Nucleation is more frequent in the case of very thin layers or inhomogeneous materials; propagation is predominant in brittle, homogeneous materials such as ceramics.

Fractures patterns resulting mostly from propagation of already formed fracture lines present a well defined hierarchy due to the sequential formation process. One such fracture pattern is the one shown in figure 1. Figure 9 shows the recovered ranks obtained with our algorithm for all the lines when the two oldest are selected. There is a partial mismatch between real and inferred hierarchy. This is in part due to the fact that when a cell is cut in two halves by a fracture, then the two halves become independent from one another and it is no longer possible to establish a temporal relation between the new fracture events within a cell and those in the neighboring one. In the case of perfect hierarchical organization (as is the case with figure 9) one could also gain information by considering the organization of angles at both extremities of a segment: the fracture line marked with \circ terminates the fracture marked with \square , indicating that this latter is actually more recent. Unfortunately, a method that considers both extremities would lose generality and could not resolve a configuration where a segment “A” is terminated by another segment “B”, the segment “B” is terminated by “C” and segment “C” is terminated by

“A”.

Once acknowledged that, depending on the characteristics of the material, some fracture patterns are mostly dominated by the nucleation of new fractures, and others by the elongation of existing ones, we want to test if our algorithm gives different classification results in one case and in the other. To this end, let us consider the crack patterns formed in three different materials: paint, desiccating clay and ceramics (figure 10 from top to bottom). The patterns were photographed with a digital camera, converted to grayscale images, high-pass filtered to remove inhomogeneities in the illumination, binarized by simple thresholding and cleaned applying a binary morphological majority filter (see [49, 50] for a review of common image processing techniques). The images of the fracture patterns were then skeletonized with a topology preserving algorithm based on distance transformation [51] to obtain a 8-connected skeleton (a skeleton where two pixels are considered to be connected if they share either a face or a corner, opposed to a 4-connected skeleton where only pixels that share a face are considered to be connected). For each skeleton pixel, we counted the number of pixels in their 8-neighborhood that also belonged to the skeleton, and all the pixels having a number of neighbors not equal to 2 were marked. All the connected sets of marked skeleton pixels were mapped into a network node. Whenever there was in the image an unmarked 8-connected path between two clusters of pixels identified as nodes we introduced an edge between the corresponding nodes. The orientation of each edge was estimated from the coordinates of the two endpoints. In a subsequent step, edges shorter than a threshold length (3 pixels) were removed and the nodes at the two endpoints merged together.

A rectangular section of the pattern is studied and all the edges crossing one side of the rectangle are selected as roots for the assignment of ranks. Figure 10 reports the statistics obtained on the three patterns, together with a snapshot of a small region of the original patterns (on the right), where the structure is colored according to the rank of the corresponding network edge.

Very different distributions are observed for the cracks formed in paint and clay, versus cracks formed in ceramics: in the former two, the lack of large scale organization is reflected into the linear increase of ranks with the topological distance from the root and the flat rank probability distribution. In fact, the junctions originating from nucleation of new fractures, whose angles are ~ 120 degrees always determine the increase of the rank of edges across the junction. The inverse of the slope of the curve fitting the data gives an indication of the length over which crack elongation proceeds: about three junctions. Conversely, for cracks formed in ceramics, the edge ranks are almost completely independent of the topological distance of edges from the roots, because of the large scale organization present in these patterns. The slope is thus close to null, but we can still see a deviation of the rank histogram toward the left of the theoretical normal

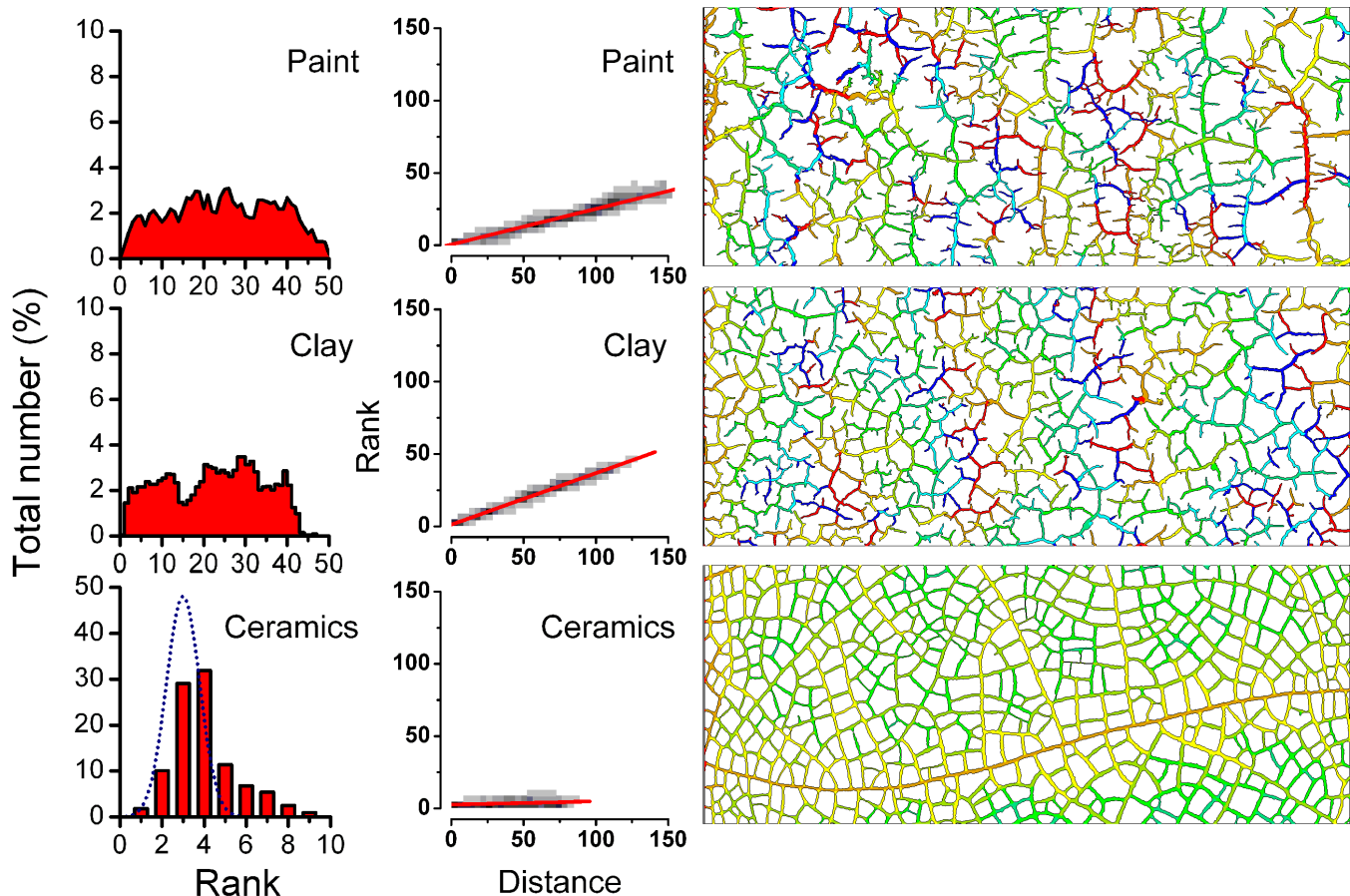


FIG. 10: Crack patterns formed in a layer of paint (top), in thin desiccating clay (middle), in the glaze of ceramics (bottom). The graphs on the left plot the rank of each network edge vs. the topological distance of the same edge from the selected roots. The images on the right are particulars of the original patterns, where the fractures have been colored according to the rank of the corresponding network edge. The same periodic rainbow colormap as in figure 4 is used. The slope of the red line fit is 0.246 for paint, 0.356 for clay and 0.022 for ceramics; $N(\bar{r})$ is 0.000 for clay and paint and 0.472 for ceramics

distribution (Fig. 10, left column, bottom). Such small deviation is probably due to the fact that analyzed region is a portion of a larger pattern and the cuts introduced by the arbitrary frame disconnected some edges from the network path that corresponds to their real rank. This also shows that rank distribution is a very sensitive measurement.

V. LEAF VENATION NETWORKS

Leaf veins in the leaves of flowering plants form characteristic patterns that can be used by botanists as keys for taxonomic identification. However this identification is done by eye and does not rely on quantitative measurements. The pattern is hierarchical, and the diameter of a vein roughly reflects its order of appearance during leaf morphogenesis, with larger veins being older than smaller ones [52]. Botanists define discrete vein orders looking at vein width at the point of branching from its parent vein: the large primary vein or midvein is continuous with the

stem vascular bundles; secondary veins branch from the primary vein; tertiary veins are defined by their narrower width where they branch from the secondary veins and so on.

We tested our ranking algorithm on the vein patterns of angiosperm leaves. The leaves were skeletonized or cleared with 10% sodium hydroxide solution and the pattern was scanned with a commercial scanner in transmission mode with a resolution superior to 2000 pixels/inch and 256 gray levels. A network representation was extracted from the images in a similar way to what described in the previous section. In the ranking procedure, the leaf stem is selected as root edge. This in agreement with its special role for both transportation and leaf morphogenesis: the leaf stem is both the source (through xylem) and the sink (through phloem) of all transportation taking place in the leaf vein network, as well as the first vein to form during leaf morphogenesis [53].

Figure 11 shows a portion of leaf of *Hymenanthera chathamica* highlighting vein ranks: veins with rank equal to 1 or 2 are shown in color in A, veins with rank

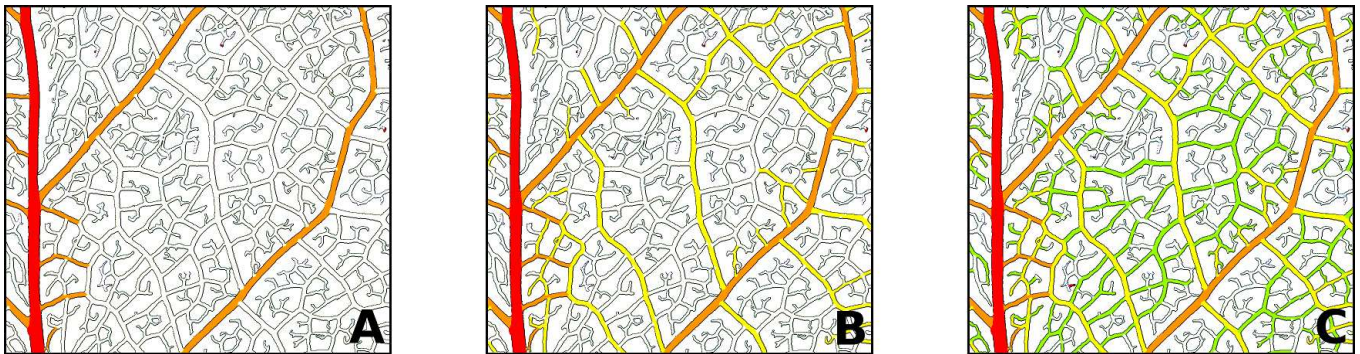


FIG. 11: **A** Vein pattern of a dicotyledon: *Hymenantha chathamica*. **A**: only the veins with rank 0 and 1 are shown in colour. **B**: only veins of rank 0,1 and 2 are colored. **C**: only veins of rank 0 to 3 are colored. (The whole leaf was analyzed, but for clarity only a small portion of the vein network is shown here).

1 to 3 are highlighted in B and veins with rank 1 to 4 in C. The classification does not take into account diameters of the veins, but only their direction. Nevertheless, the results of classification match well the diameter of the veins: from the figure, we can see that veins marked with higher ranks have in general smaller size (which roughly corresponds to say that they have appeared later). In this sense, we also recover the vein patterns as derived from the botanical classification. This is coherent with the hypothesis that the older veins are not only larger but also straighter, as can be derived from relation existing between vein sizes and junction angles [33]. Some small veins attached to the main vein are given a small rank, while one would intuitively ascribe them to a higher rank. This illustrates well the non complete reversibility of the fragmentation process: for each vein we can infer the order of appearance with respect to the parent vein, but not the exact age. Technically, also the botanical classification presents the same problem as these veins have smaller diameters than the parent vein.

Going to the statistics of segment percentages and edge rank vs. distance, we plot them in figure 12 for both the *Hymenantha chathamica* (*Hc*) leaf and for a leaf of *Ficus religiosa* (*Fr*). The *Hc* network is about one magnitude order smaller than the *Fr*. However, both networks are hierarchical: the distribution of segment histogram is peaked close to the theoretical value and the slope of rank vs. distance is close to zero (please note the x- and y- axes scales).

The larger *Fr* pattern is very close to the perfect hierarchical pattern, while there is a slight deviation for *Hc* rank distribution: it is still a Gaussian but shifted to higher values. Contrary to the previous case, it cannot be ascribed to boundary effects as the whole leaf with the boundary veins is treated, nor to a simple small number of veins, as the distribution is already very well defined. This shift might be ascribed to the different plasticity of the veins during their maturation, and that the connection angle evolves a little, but not enough to disrupt the hierarchy. More measurements should be made to check if this shift is due to the difference in species or to

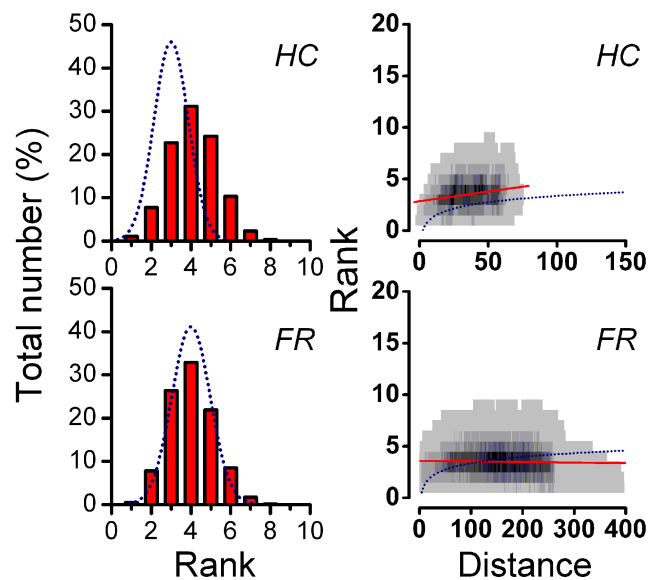


FIG. 12: Top: Segement and edge statistics for *Hymenantha chathamica* (*Hc*, top) and *Ficus religiosa* (*Fr*, bottom). Network size is ~ 12000 nodes for *Hymenantha* and ~ 130000 for *Ficus*. The slope of the red line fit is 0.019 for *Hc* and 0.000 For *Fr*. $N(\bar{r})$ is 0.456 for *Hc* and 0.999 for *Fr*

the different maturation of the leaves depending on their sizes.

VI. URBAN STREET PATTERNS

The growth of urban street networks is a complex process determined by a series of historical events and involving feed-back and regulation from global network processes, such as traffic and transportation. However, in a first approximation, the general form of these patterns can be described in terms of simple models where new streets appear over time with no reorganisation [16, 54, 55]. Within such models, the first streets will

connect the first houses to the country. As the urban pattern grows, new streets will bifurcate from existing ones in the direction of not yet urbanized areas, or to join already existing streets. Hence, the process of growth of urban streets would share similarities with the growth of fracture patterns [34], which justifies to assign ranks to streets in a similar way.

We here test our ranking method on two towns Cordoba (Spain) and Venice (Italy) to look at the distribution of statistics for the two towns. In both cases we choose the perimeter of the town as root for the rank computation. (The shores of Venice and the highway ring around Cordoba).



FIG. 13: Cordoba map, edges are colored according to their rank.

Figure 13 displays a map of the town of Cordoba, where each edge is colored according to its rank. The brighter region in the figure corresponds to the historical city centre. Almost all the edges with highest rank appear to fall inside this region. Higher ranks often are the mark of lack of global organization. It would be interesting to explore further if higher ranks correspond to parts of town that developed in a period of more self-organized, organic growth (e.g. periods when the central power was weaker). Overall, the histogram of segments of different ranks (reported in fig. 14 top, left) is still compatible with that of a hierarchical network, as those found in the previous example. The distribution of edge ranks vs. edge distance from the root edges is nearly flat, with a slight slope that can likely be ascribed to the small size of the network.

When the same analysis is carried on the street pattern of Venice, a quite different behavior is found: segments rank up to much higher values, suggesting an absence of large scale organization in this street pattern (fig. 14, middle column). This does not seem to be a pure artifact of our method, but agrees with other elements of the organization of Venice, where streets are not the principal

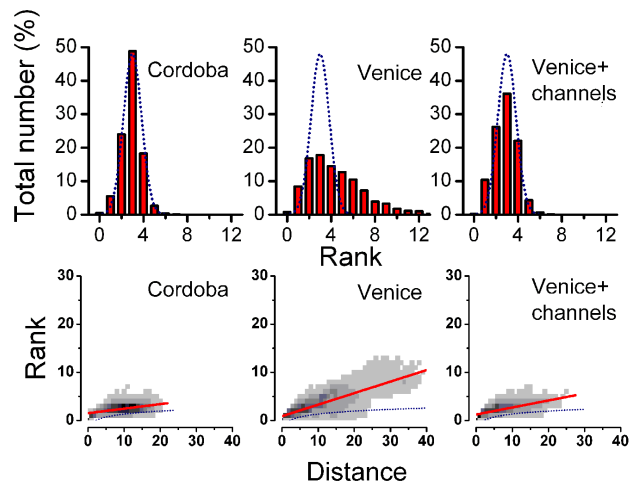


FIG. 14: Top: Histogram of the number of segments in Cordoba street pattern, Venice street pattern and Venice street and channel pattern. Bottom: rank of network edges vs. their topological distance from the root edges. The slope of the red curve is 0.094 for Cordoba, 0.239 for Venice, and 0.146 when also the channels are considered in the network. $N(\bar{r})$ is 0.991 for Cordoba, 0.985 for Venice with channels and 0.259 for Venice without channels.



FIG. 15: Direct access to the channel network from a house in Venice

element of organization of the town. This is reflected, for instance, in the fact that still today houses and buildings are not numbered according to their position along a street, but numbering follows a subdivision by districts (“sestieri”).

Interestingly, when for Venice one considers the transportation system including both streets and channels, the rank distribution gets closer to one of a hierarchical network, with histogram of segment numbers limited to ~ 5 ranks and less steep distribution of edge ranks vs. distances (fig. 14, right). This reveals that the channels are the original part of the transportation system, and the

origin of the town organization. The houses were first built along the channels with direct access to them (fig. 15), and the streets appeared in the channel delimited islands, as secondary divisions for inland house access. Thus removing the channels for the analysis is removing the large coherent structure, having a direct visible impact on the rank distribution shape. On the contrary, with the channels included, the hierarchical structure of successive divisions is recovered. So, the rank analysis has the potential to show some peculiarities of specific towns at the same time pointing to the possible reasons for these peculiarities.

VII. CONCLUSIONS

In this article we defined a new method to analyze spatial networks with loops and define quantitative measurements. The need to characterize quantitatively the form (and likely morphogenesis) of net-like patterns motivated us to introduce a procedure for assigning ranks to all the edges of the pattern and group several edges into segments. Using a local spatial characteristics, the branching angles, we are able to quantify the large scale coherence of the pattern. In the examples of the present paper, the root of the analysis is decided arbitrarily (from intuitive clues). However, for many purposes one does not need to define a root for computation and can compute more classical network parameters directly on the weighted line graph G_D .

The first measurement we propose, the rank distribution, is a very sensitive indicator of the existence of a large scale spatial coherence and hierarchical subdivisions. When this large scale coherence is lost, the second measurement quantifies the size over which organization persists, up to the point of purely local organization. When tested on lattice models, these measurements show a continuous but sharp transition between two types of network, one with large scale coherence and one with purely a local organization.

The method is efficient on different real patterns taken from various origins, from fractures to leaf venation and urban streets. The obtained measures show the poten-

tiality to discriminate between patterns with hierarchical history of growth and patterns grown out of more local rules. It is perfectly clear for fracture patterns, where the two cases of many locally generated fractures that reconnect and few fractures propagating on large distance can be clearly distinguished. For leaf venation pattern, the method clearly reveals a hierarchical growth mechanism. In addition, the rank assigned to network segments correlates to some extent with the temporal order of appearance of the same segments, and hence the measure is informative on the process of growth itself. The matching between ranks and order of appearance however is not perfect, and the information provided by the ranks should be complemented from other sources for individual systems. For instance, with leaf veins one could consider both ranks and vein diameter to obtain a better classification of veins into discrete orders.

This analysis is also sensitive on town streets, and is able to reveal the particular organization of streets in Venice, whose structure can be explained as a secondary construction from the channels. The town structures is otherwise coherent with that of a sequential sub-division pattern, indicating some underlying logic in its development.

We think the method can be generally applied to different types of patterns, revealing not only their structure but also in part their history of growth. In the present paper, we build the classification from local angle information. More generally, however, any other local information can be used, for instance the size of the connecting element, to construct a similar hierarchy. It is thus a new, general and efficient way to analyze networks with loops and group patterns of very diverse origins into the same structure and development classes.

VIII. ACKNOWLEDGEMENTS

We are grateful to Fabien Picarougne for comments and advice on the C++ implementation of the algorithm. This work was supported by ANR-06-BYOS-0008. The computer code used for this paper is available upon request from the authors.

-
- [1] R. E. Horton. Erosional development of streams and their drainage basins: Hydrophysical approach to quantitative morphology. *Geological Society of America Bulletin*, 56:275–370, (1945).
 - [2] A. N. Strahler. Dynamic basis of geomorphology. *Geological Society of America Bulletin*, 63:923–938, (1952).
 - [3] P. S. Dodds, D. H. Rothman. Geometry of river networks. I. Scaling, fluctuations, and deviations. *Phys Rev E* 63:016115. doi:10.1103/PhysRevE.63.016115 (2000)
 - [4] P. S. Dodds and D. H. Rothman. Geometry of river networks. II. Distribution of component size and number. *Phys Rev E* 63:016116. doi:10.1103/PhysRevE.63.016116 (2000a)
 - [5] Dodds PS, Rothman DH. Geometry of river networks. III. Characterization of component connectivity. *Phys Rev E* 63:016117. doi:10.1103/PhysRevE.63.016117 (2000b)
 - [6] J. D. Pelletier and D. L. Turcotte. Shapes of river networks and leaves: are they statistically similar? *Philos Trans R Soc Lond B* 355:307311. doi:10.1098/rstb.2000.0566 (2000)
 - [7] K.N. Ganeshaiah and T. Veena. Topology of the foraging trails of *Leptogenys processionalis* why are they branched? *Behav Ecol Sociobiol* 29:263270 (1991)
 - [8] S. Boccaletti, V. Latora, Y. Moreno, M. Chavez, and

- D. U. Hwang. Complex networks: Structure and dynamics. *Physics Reports - Review Section of Physics Letters*, 424:175–308, (2006).
- [9] L. Da Fontoura Costa, F. A. Rodrigues, G. Travieso, and P. R. Villas Boas. Characterization of complex networks: A survey of measurements. *Adv. Phys.*, 56:167, (2007).
- [10] M. Barthelemy. Spatial Networks arXiv:1010.0302v2 (2010)
- [11] J. Buhl, J. Gautrais, N. Reeves, R. V. Solé, S. Valverde, P. Kuntz, and G. Theraulaz. Topological patterns in street networks of self-organized urban settlements. *European Physical Journal B*, 49:513–522, (2006).
- [12] P. Crucitti, V. Latora, and S. Porta. Centrality measures in spatial networks of urban streets. *Phys. Rev. E*, 73:036125, (2006).
- [13] S. Scellato, A. Cardillo, V. Latora, and S. Porta. The backbone of a city. *European Physical Journal B*, 50:221–225, (2006).
- [14] A. Cardillo, S. Scellato, V. Latora, and S. Porta. Structural properties of planar graphs of urban street patterns. *Phys. Rev. E*, 73:066107, (2006).
- [15] S. Porta, P. Crucitti, and V. Latora. The network analysis of urban streets: A dual approach. *Physica A*, 369:853–866, (2006).
- [16] M. Barthelemy and A. Flammini. Modeling urban street patterns. *Phys. Rev. Lett.*, 100:138702, (2008).
- [17] B. Jiang and C. Claramunt. Topological analysis of urban street networks. *Environment and Planning B - Planning and Design*, 31:151–162, (2004).
- [18] B. A. N. Travencolo and L. da Fontoura Costa. Outward accessibility in urban street networks: Characterization and improvements, arXiv.org:0802.3665 (2008).
- [19] M. T. Gastner and M. E. J. Newman. Shape and efficiency in spatial distribution networks. *Journal of Statistical Mechanics: Theory and Experiment*, 2006:P01015, (2006).
- [20] J. Buhl, K. Hicks, E. Miller, S. Persey, O. Alinvi, and D. Sumpter. Shape and efficiency of wood ant foraging networks. *Behavioral Ecology and Sociobiology*, 63(3):451–460, (2009).
- [21] J. Buhl, J. Gautrais, R. V. Solé, P. Kuntz, S. Valverde, J. L. Deneubourg, and G. Theraulaz. Efficiency and robustness in ant networks of galleries. *European Physical Journal B*, 42:123–129, (2004).
- [22] A. Perna, C. Jost, E. Couturier, S. Valverde, S. Douady, and G. Theraulaz. The structure of gallery networks in the nests of *Cubitermes* spp. revealed by x-ray tomography. *Naturwissenschaften*, 95:877–884, (2008).
- [23] A. Perna, C. Jost, S. Valverde, J. Gautrais, G. Theraulaz, and P. Kuntz. The topological fortress of termites. In *Bio-inspired Computing and Communication, LNCS*, 5151, 165–173, (2008).
- [24] A. Perna, S. Valverde, J. Gautrais, C. Jost, R. Solé, P. Kuntz, and G. Theraulaz. Topological efficiency in three-dimensional gallery networks of termite nests. *Physica A*, 387:6235–6244, (2008).
- [25] S. Valverde, B. Corominas-Murtra, A. Perna, P. Kuntz, G. Theraulaz, and R. V. Solé. Percolation in insect nest networks: Evidence for optimal wiring. *Phys. Rev. E*, 79:066106, (2009).
- [26] L. da Fontoura Costa, M. Palhares Viana, and M. E. Beletti. The complex channel networks of bone structure. *Applied Physics Letters*, 88:033903, (2006).
- [27] M. Palhares Viana, E. Tanck, M. E. Beletti, and L. da Fontoura Costa. Modularity and robustness of bone networks. *Molecular BioSystems*, 5:255, (2009).
- [28] D. P. Bebber, J. Hynes, P. R. Darrah, L. Boddy, and M. D. Fricker. Biological solutions to transport network design. *Proc. Roy. Soc B*, 274:2307–2315, (2007).
- [29] A. Fronczak, P. Fronczak, J. A. Holyst. Average path length in random networks. *Phys. Rev. E*, 70:056110, (2004)
- [30] D. Watts. *Small worlds: the dynamics of networks between order and randomness* Princeton University Press, Princeton, N.J (1999)
- [31] D. L. Weaire and S. Hutzler. *physics of foams*. Clarendon Press, Oxford, 1999.
- [32] D’Arcy Wentworth Thompson. *On Growth and Form: The Complete Revised Edition*. Dover, 1992.
- [33] S. Bohn, B. Andreotti, S. Douady, J. Munzinger, and Y. Couder. Constitutive property of the local organization of leaf venation networks. *Phys Rev E*, 65:061914, (2002).
- [34] S. Bohn, S. Douady, and Y. Couder. Four sided domains in hierarchical space dividing patterns. *Phys. Rev. Lett.*, 94:054503, (2005).
- [35] S. Lämmer, B. Gehlsen, and D. Helbing. Scaling laws in the spatial structure of urban road networks. *Physica A*, 363:89 – 95, (2006).
- [36] S. Bohn, L. Pauchard, and Y. Couder. Hierarchical crack pattern as formed by successive domain divisions. *Phys. Rev. E*, 71:046214, (2005).
- [37] B. Hillier and J. Hanson. *The Social Logic of Space*. Cambridge University Press, Cambridge (1984).
- [38] B. Hillier, A. Penn, J. Hanson, T. Grajewski, and J. Xu. Natural movement: or, configuration and attraction in urban pedestrian movement. *Environment and Planning B: Planning and Design*, 20:29–66, (1993).
- [39] C. Ratti. Urban texture and space syntax: some inconsistencies. *Environment and Planning B: Planning and Design*, 31:513–516 (2004).
- [40] M. Rosvall, A. Trusina, P. Minnhagen, and K. Sneppen. Networks and cities: An information perspective. *Phys. Rev. Lett.*, 94:028701, (2005).
- [41] V. Kalapala, V. Sanwalani, A. Clauset, and C. Moore. Scale invariance in road networks. *Phys. Rev. E*, 73:026130, (2006).
- [42] R. Bulkeley. Part of a Letter from Sir R. B. S. R. S. to Dr. Lister, concerning the Giants Causway in the County of Antrim in Ireland. *Phil. Trans. R. Soc. London*, 17:708–710, (1693).
- [43] T. Aste and D. Weaire. *The Pursuit of Perfect Packing*. IoP/Bookmark, (2000).
- [44] A. Aydin and J. M. Degraff. Evoluton of Polygonal Fracture Patterns in Lava Flows. *Science*, 239(4839):471–476, (1988).
- [45] E. A. Jagla and A. G. Rojo. Sequential fragmentation: The origin of columnar quasihexagonal patterns. *Phys. Rev. E*, 65(2):026203, (2002).
- [46] K. A. Shorlin, J. R. de Bruyn, M. Graham, and S. W. Morris. Development and geometry of isotropic and directional shrinkage-crack patterns. *Phys. Rev. E*, 61(6):6950–6957, (2000).
- [47] H.-J. Vogel, H. Hoffmann, and K. Roth. Studies of crack dynamics in clay soil: I. experimental methods, results, and morphological quantification. *Geoderma*, 125:203 – 211, (2005).
- [48] K. B. Toga and B. Erdem Alaca. Junction formation

- during desiccation cracking. *Phys. Rev. E*, 74(2):021405, (2006).
- [49] R. C. Gonzalez and R. E. Woods. *Digital Image Processing*. Prentice Hall, Upper Saddle River, New Jersey, (2002).
- [50] J. R. Parker. *Algorithms for Image Processing and Computer Vision*. John Wiley & Sons, New York, NY, (1997).
- [51] Ta-Chih Lee, Rangasami L. Kashyap, and Chong-Nam Chu. Building skeleton models via 3-d medial surface/axis thinning algorithms. *CVGIP: Graph. Models Image Process.*, 56(6):462–478, (1994).
- [52] T. Nelson and N. Dengler. Leaf vascular pattern formation. *Plant Cell*, 9(7):1121–1135, (1997).
- [53] L. Taiz and E. Zeiger. *Plant Physiology, Fifth Edition*. Sinauer Associates, Inc. (2010).
- [54] M. Barthélemy and A. Flammini. Co-evolution of density and topology in a simple model of city formation. *Networks and Spatial Economics*, 9(3):401–425, Sep 2009. 10.1007/s11067-008-9068-5.
- [55] T. Courtat, C. Gloaguen, S. Douady. Mathematics and Morphogenesis of the City: A Geometric Approach. arXiv:1010.1762v2